Published in final edited form as:
Nature. 2008 February 14; 451(7180): 830–834. doi:10.1038/nature06529.

A modular switch for spatial Ca^{2+} selectivity in the calmodulin regulation of CaV channels

Ivy E. Dick[*], **Michael R. Tadross**[*], **Haoya Liang**, **Lai Hock Tay**, **Wanjun Yang**, and **David T. Yue**[‡]

Calcium Signals Laboratory, Departments of Biomedical Engineering and Neuroscience, The Johns Hopkins University School of Medicine, Ross Building, Room 713, 720 Rutland Avenue, Baltimore, MD 21205

Abstract

Ca^{2+}/calmodulin-dependent regulation of voltage-gated Ca_V1-2 Ca^{2+} channels exhibits extraordinary modes of spatial Ca^{2+} decoding and channel modulation[1–6], vital for many biological functions[6–9]. A single calmodulin (CaM) constitutively associates with the channel carboxy tail[3,10–13], and Ca^{2+} binding to the C- and N-terminal lobes of CaM can each induce distinct channel regulations[2,14]. As expected from close channel proximity, the C-lobe responds to the ~100 μM Ca^{2+} pulses driven by the associated channel[15,16], a behavior defined as 'local Ca^{2+} selectivity.' Conversely, all prior observations indicate that the N-lobe somehow senses the far weaker signals from distant Ca^{2+} sources[2,3,17,18]. This 'global Ca^{2+} selectivity' satisfies a general signaling requirement, enabling a resident molecule to remotely sense cellular Ca^{2+} activity, which would otherwise be overshadowed by Ca^{2+} entry through the host channel[5,6]. Here, we report that the spatial Ca^{2+} selectivity of N-lobe CaM regulation is not invariably global, but can be switched by a novel Ca^{2+}/CaM binding site within the amino terminus of channels (*NSCaTE*, N-terminal Spatial Ca^{2+} Transforming Element). Native $Ca_V2.2$ channels lack this element, and display N-lobe regulation with a global selectivity. Upon introducing *NSCaTE* into these channels, spatial Ca^{2+} selectivity transforms from a global to local profile. Given this effect, we examine $Ca_V1.2$/$Ca_V1.3$ channels, which naturally contain *NSCaTE*, and find that their N-lobe selectivity is indeed local. Disruption of this element produces a global selectivity, confirming the native function of *NSCaTE*. Thus differences in spatial selectivity between advanced Ca_V1 and Ca_V2 channel isoforms are explained by the presence or absence of *NSCaTE*. Beyond functional effects, the position of *NSCaTE* on the channel amino terminus indicates that CaM can bridge the amino and carboxy termini of channels. Finally, the modularity of *NSCaTE* offers practical means to understand the basis of global Ca^{2+} selectivity[19].

Figs. 1a, b display a prototypic example of global Ca^{2+} regulation induced by Ca^{2+} binding to the N-lobe of CaM, here driving Ca^{2+}-dependent inactivation (CDI) of $Ca_V2.2$ channels[3]. Upon channel activation by a depolarizing voltage step (Fig. 1a), this CDI manifests as the accelerated decay of Ca^{2+} (middle, red trace) versus Ba^{2+} current (black trace). The baseline

[‡]To whom correspondence should be addressed Calcium Signals Laboratory, Departments of Biomedical Engineering and Neuroscience, The Johns Hopkins University School of Medicine, Ross Building, Room 713, 720 Rutland Avenue, Baltimore, MD 21205, voice: (410) 955-0078, fax: (410) 955-0549, dyue@bme.jhu.edu.
[*]Contributed equally

decay in Ba^{2+}, which binds poorly to CaM[2], reflects a separate voltage-dependent inactivation process[7]. In population data (right), the fraction of peak Ca^{2+} current remaining after a 300 ms depolarization, r_{300}, is a U-shaped function of voltage (red circles), providing a hallmark of CDI[20]. The corresponding Ba^{2+} relation (black circles) shows a weak monotonic decline, and the difference between Ca^{2+} and Ba^{2+} relations (f_{300}) quantifies pure CDI[20]. In accord with a thus far invariant rule[3,6], N-lobe regulation of Ca^{2+} channels is selective for global Ca^{2+} elevation arising from spatially distant sources. Such global crosstalk is permitted under modest intracellular Ca^{2+} buffering[18] that approximates physiological conditions (Fig. 1a, left, shading with 0.5 mM EGTA). Thus, strong buffering that localizes Ca^{2+} to channel nanodomains[15,16] (Fig. 1b, left, small hemisphere in 10 mM BAPTA) nearly eliminates CDI (Fig. 1b, middle and right).

Previous splice variations, mutations, and chimeras have at best altered the strength of such CDI[2,3,21], making global Ca^{2+} preference appear immutable. Here, however, when the amino terminus of $Ca_V1.2$ channels (NT_C) was substituted into $Ca_V2.2$, the resulting ‘cBBBBb’ chimera exhibited strong N-lobe CDI in high buffering (Fig. 1c, Supplementary Information 1.1). Introducing NT_C into $Ca_V2.1$ produced an analogous result (data not shown), thus generalizing the effect across the Ca_V2 family. This conversion to local Ca^{2+} selectivity is unprecedented, especially given the preponderance of known structural determinants for CDI on the carboxy termini of channels[22].

To explore the basis of this effect, we undertook progressive amino-terminal deletions from the NT_C segment within the cBBBBb chimera. Deleting the first 81 residues (Δ82cBBBBb) completely spared CDI in high buffering (Fig. 1d, top, left), where the gray trace shows the full-length NT_C profile. By contrast, removing just one more residue (82W) significantly reduced CDI (Fig. 1d, top, middle), and additional deletion further suppressed CDI (Fig. 1d, top, right). Explicit correlation of CDI strength with NT_C deletion corroborated these trends (Fig. 1d, bottom, left axis, circles), localizing the impact to a short contiguous region (yellow highlight).

What could be the essential mechanistic ingredient of this locus? We reasoned that this segment might orchestrate special molecular interactions with cytoplasmic channel loops or modulatory ligands, and thus probed for such associations using a live-cell FRET two-hybrid assay[13]. Using this approach, with EYFP fused to CaM (EYFP–CaM), and ECFP to various portions of NT_C or the $Ca_V2.2$ amino terminus (NT_B), we found a unique ability of NT_C to bind Ca^{2+}/CaM within the intracellular milieu of HEK293 cells (Fig. 1e). To start, NT_B failed to display FRET interaction with CaM, either in Ca^{2+}-free or Ca^{2+}-bound states (Fig. 1e, middle column, topmost bars). Specifically, the optical parameter *FR* was ~1, signifying the absence of FRET[13]. By contrast, NT_C clearly interacted with Ca^{2+}/CaM (*FR* ~2), but not apoCaM (Ca^{2+}-free CaM). Trisection of NT_C localized Ca^{2+}/CaM binding to the middle third (Fig. 1e, middle column, residues 67–131), and further deletions identified a sharp decrease in FRET upon removal of W82 (Supplementary Information 1.2). Since *FR* depends on the fractional binding between interacting partners, cell-to-cell variation in expression permitted resolution of binding curves, each specifying a relative dissociation constant $K_{d,EFF}$[13] (Fig. 1e, right column, arrow). Alignments of these NT_C fragments and their $K_{d,EFF}$ values (Fig. 1d, squares, Supplementary Information 1.2) localized a CaM-

binding segment that coincides well with the critical CDI segment (Fig. 1d, yellow highlight). Notably, a W82A point mutation suppressed Ca^{2+}/CaM interaction with NT_C (Fig. 1f), fitting with the drop in CDI of the corresponding channel truncation (Fig. 1d, top row, middle). Thus, the transformation of spatial Ca^{2+} selectivity correlates with a novel Ca^{2+}/CaM interaction site within NT_C.

This connection was deepened in two ways (Fig. 2). First, the *in situ* FRET approach was confirmed by *in vitro* assays, pairing purified Ca^{2+}/CaM with a synthetic peptide (SWQAAIDAARQAKLMGSA) spanning the key NT_C binding region. Without peptides, CaM migrated rapidly under non-denaturing PAGE[2] (Fig. 2a, left gel, lane 1, open triangle). When fully complexed with the IQ domain peptide of $Ca_V2.1$ (IQ_A), CaM exhibited a known slowing of mobility[2] (lane 2, filled triangle). Increasing $NT_{C\text{-}peptide}$ produced progressive conversion to the faster mobility species (lanes 3–8), indicating competitive binding to CaM. By contrast, a mutant W82A peptide ($NT_{C\text{-}peptide\text{-}(W82A)}$, right gel) was unable to bind CaM. More quantitatively, $NT_{C\text{-}peptide}$ depressed the emission spectrum of dansylated CaM (Fig. 2b, inset), allowing resolution of a 1:1 binding curve with a K_d of 1.2 μM (Fig. 2b, black symbols). $NT_{C\text{-}peptide\text{-}(W82A)}$ exhibited no such interaction (Fig. 2b, open symbols). These *in vitro* assays established direct Ca^{2+}/CaM binding to the NT_C core region.

Second, further in-depth mapping refined the correlation between spatial Ca^{2+} selectivity and CaM binding to NT_C. Alanine point mutations were introduced into the NT_C domain of cBBBBb channels, targeting key sites inferred from a preliminary report[19]. These manipulations reduced CDI (in high buffering) with the rank order: W82A > I86A > R90A (Fig. 2c). Reassuringly, these changes in CDI (f_{300}) correlated closely with the relative dissociation constant ($K_{d,EFF}$) for CaM interaction with corresponding mutant NT_C peptides, as determined by FRET (Fig. 2d, Supplementary Information 2.1). Given the strong function and affiliation with CaM binding to the core NT_C locus, we named this element *NSCaTE* (Fig. 2c, top N-terminal Spatial Ca^{2+} Transforming Element).

While this module impacts chimeric channels, does *NSCaTE* function within naturally occurring channels? Alignments of various Ca_V1-2 Ca^{2+} channels (Fig. 3a) revealed that *NSCaTE* is present not only in $Ca_V1.2$ (α_{1C}), but also $Ca_V1.3$ (α_{1D}). Our attention was foremost drawn to *NSCaTE* in $Ca_V1.3$, as these channels exhibit two distinct and robust forms of CDI, each selectively triggered by Ca^{2+} binding to a different lobe of CaM[14]. As a preliminary test for the functionality of the $Ca_V1.3$ *NSCaTE*, we checked for Ca^{2+}/CaM interaction (Fig. 3b). FRET assays showed selective Ca^{2+}/CaM interaction with the midsection of the $Ca_V1.3$ amino terminus (Fig. 3b, NT_D-(35–94)), yielding a $K_{d,EFF}$ on par with NT_C analogs (Fig. 1e). Consistent with W82A effects in NT_C (Fig. 1f), mutating the analogous tryptophan in NT_D (NT_D-W44A-(35–94)) eliminated Ca^{2+}/CaM interaction (Fig. 3b, Supplementary Information 3.1). Substituting NT_D into $Ca_V2.2$ (yielding the dBBBBb chimera) also produced strong CDI in high buffering (Fig. 3c, Supplementary Information 3.1), confirming the transforming capacity of the $Ca_V1.3$ *NSCaTE*.

Encouraged by these preliminary results, we asked whether the intrinsic *NSCaTE* imparts local selectivity to the native $Ca_V1.3$, contrary to the current dogma that the N-lobe invariably senses global Ca^{2+}. In $Ca_V1.3$, the N-lobe form of CDI can be isolated by

coexpresing a mutant CaM (CaM_{34}) in which Ca^{2+} binding is restricted to the N-lobe[2,20]. Thus far, such CDI has only been studied under modest Ca^{2+} buffering[14]. Here, even under high buffering, N-lobe CDI was pronounced (Fig. 3d, top row). More telling, a W44A mutation within $Ca_V1.3$ nearly eliminated this CDI (middle row), as did deletion of this region (Supplementary Information 3.2). To exclude indiscriminate disruption of CDI, we confirmed that CDI resurfaced under modest buffering permissive of global signaling (Fig. 3d, bottom row, Supplementary Information 3.2). Importantly, CDI was entirely CaM-mediated under reduced buffering[14] (Supplementary Information 3.3); and C-lobe CDI was unaffected by like mutations[19]. Hence, the native $Ca_V1.3$ *NSCaTE* endows N-lobe CDI with a local selectivity, and reducing Ca^{2+}/CaM binding to *NSCaTE* switches this selectivity towards a global profile.

Returning to native $Ca_V1.2$, coarse identification of Ca^{2+}/CaM binding to the amino terminus of these channels has been reported, but the functional consequences have been unclear[23]. In particular, the CaM-mediated CDI of these channels has been attributed only to the C-lobe of CaM[7,20]; apparently absent has been an N-lobe form of CDI, the target of *NSCATE* effects. Here, however, upon co-transfection of $Ca_V1.2$ with CaM_{34}, to fully isolate a potential N-lobe component, small but unmistakable CDI is seen during prolonged 1-sec depolarization, even in high buffering (Fig. 3e, top row). As well, a W82A mutation abolished this CDI (middle row), but spares it under global Ca^{2+} signaling (bottom row). A more drastic deletion of the native *NSCaTE* produced an identical effect (Supplementary Information 3.4). Again, the globally signaled CDI remains entirely CaM dependent (Supplementary Information 3.5). Hence, *NSCaTE* functions similarly in native $Ca_V1.2$ and $Ca_V1.3$; the weaker N-lobe CDI of $Ca_V1.2$ is expected from its lower open probability[19,24]. These results generalize the lessons of chimeric channels to the operation of native channels and constitute the first examples where the N-lobe of CaM shows local Ca^{2+} selectivity.

In all, the traditionally global spatial Ca^{2+} selectivity of channel regulation by the N-lobe[3,6] is not invariant, but can be transformed towards a local selectivity by *NSCaTE*, a novel Ca^{2+}/CaM binding site unrecognized by current motif-detection algorithms[25]. Four perspectives emerge. First, the presence of *NSCaTE* in $Ca_V1.2$ and $Ca_V1.3$—along with its absence in Ca_V2 channels—underlies the contrasting spatial Ca^{2+} preferences of N-lobe CDI between these two channel clades (Fig. 4a). Previously, N-lobe regulation had been viewed as always having a global Ca^{2+} selectivity[3,6], which is true for Ca_V2 channels (Fig. 4b). We now recognize that the analogous N-lobe CDI of $Ca_V1.2$/$Ca_V1.3$ channels[14] exhibits local selectivity, owing to an intrinsic *NSCaTE* (Fig. 4c). Second, *NSCaTE* promises vital adjustments of spatial selectivity in diverse biological contexts. *NSCaTE* would customize $Ca_V1.2$/1.3 regulation for local Ca^{2+} signaling in cardiac dyads[4,7], and for neuronal Ca^{2+} entry whose precise regulation is essential for long-term synaptic plasticity[26,27]. Of further intrigue, a naturally occurring $Ca_V1.2$ splice variant features a premature stop codon just after the channel amino terminus[21]. The predicted protein product contains *NSCaTE*, and may exert a dominant negative effect. Although coexpressing NT_C and $Ca_V1.3$ left CDI unchanged in HEK293 cells (data not shown), additional mechanisms may exist in native tissues to render this splice product active. Third, unlike most functional motifs, which are pervasive from bacteria through advanced mammals[25], *NSCaTE* is only

found in a subset of Ca_V1 channels from advanced species (Fig. 4a, red), and in multiple bacterial proteins (Supplementary Information 4). A prokaryotic *NSCaTE* from *Xanthomonas* may in fact bind endogenous CaM-like molecules (Supplementary Information 4), hinting that channel and bacterial motifs share a common heritage. Finally, *NSCaTE* furnishes valuable structural and mechanistic insights. For structure, we deduce that CaM can bridge the carboxy and amino termini of $Ca_V1.2/Ca_V1.3$ channels (Fig. 4c, right), as follows. This study establishes Ca^{2+}-bound N-lobe interaction with *NSCaTE* on the channel amino terminus. By contrast, prior reports emphasize that regulation by the C-lobe involves its Ca^{2+}-bound and Ca^{2+}-free interactions with the channel carboxy terminus[12,20,28]. Moreover, a single resident CaM orchestrates both C- and N-lobe regulation[10,11], where both coexist in $Ca_V1.2/Ca_V1.3$ channels[14,20]. Finally, channel amino and carboxy termini are in close proximity, and move with channel gating[29]. Hence, this bridging appears probable, expanding a theme where the lobes of CaM crosslink separate parts of a molecule[30]. As for mechanism, the modularity of *NSCaTE* indicates that spatial Ca^{2+} preference is not hopelessly intertwined within holochannel structure. Manipulating this compact element promises valuable insights into the elusive mechanism underlying spatial Ca^{2+} selectivity[6,19].

Methods

Molecular Biology

The $\alpha_{1cBBBBb}$ subunit was the published $\alpha_{1cBBBBb}$/pcDNA3 construct[31]. PCR was used to truncate the amino terminus of this construct: the forward primer, containing a unique EcoRI site and Kozak start, determined the extent of truncation; the reverse primer annealed downstream of a unique AgeI site. PCR fragments were ligated into $\alpha_{1cBBBBb}$/pcDNA3 via EcoRI/AgeI. Mutations to *NSCaTE* were introduced into the $\alpha_{1\Delta 78cBBBBb}$ truncation construct (starts with 78th residue of α_{1C}), using forward primers as above, but containing desired mutations. For chimeric $\alpha_{1dBBBBb}$, PCR introduced a silent and unique BsiWI site at residue 83 of α_{1B}/pcDNA3, yielding α_{1B}_BsiWI$^+$. The amino terminus of α_{1D}[32] was PCR amplified, then ligated into unique EcoRI and BsiWI sites of α_{1B}_BsiWI$^+$, yielding $\alpha_{1dBBBBb}$. The α_{1B} ($Ca_V2.2$) used here is a variant of the human α_{1B} reported previously[33]; it is identical but for V354M and R369S variations. This variant backbone was used for all constructs, including $\alpha_{1dBBBBb}$ and the previously published $\alpha_{1cBBBBb}$/pcDNA3[31]. For completeness, we confirmed that transforming *NSCaTE* effects were also present using the more common α_{1B} backbone for $\alpha_{1cBBBBb}$ and $\alpha_{1dBBBBb}$. A 141-residue amino-terminal truncation of the $Ca_V1.2$ α_{1C} subunit ($\alpha_{1C[NT\Delta]}$) was generated by PCR amplifying residues 142–611 from α_{1C}[34], followed by ligation into the parental α_{1C} via unique KpnI and StuI sites. A 44-residue amino-terminal truncation of the $Ca_V1.3$ α_{1D} subunit ($\alpha_{1D[NT\Delta]}$) was similarly constructed by PCR amplifying residues 45–180 from α_{1D}[32], followed by ligation into α_{1D} via unique NheI and BsiWI sites. The mutant $\alpha_{1C[W82A]}$ was made by PCR amplifying α_{1C} residues 1–87, using a reverse primer containing a W82A mutation. This product was ligated into α_{1C} via unique HindIII and ClaI sites. The mutant $\alpha_{1D[W44A]}$ subunit was as described[19].

For FRET, all CFP–$NT_{B/C/D}$ constructs were made by PCR of desired segments of $\alpha_{1cBBBBb}$ or α_{1D}, followed by substitution of CaM_{WT} in a published CFP–CaM_{WT}/$pcDNA_3$ clone[13], using unique Not I and Xba I sites. For CFP fusion to the *NSCaTE* of the TonB Dependent Receptor (TBDR, amino acids 464–484 of YP_242632.1), annealed synthetic primers encoding this motif (mammalian optimized) were ligated into unique NotI/XbaI sites of CFP–CaM_{WT}/$pcDNA_3$. Throughout, all PCR amplified segments were fully verified by sequencing.

Electrophysiology

HEK293 cells were transiently transfected using a calcium phosphate protocol[20]. Cells were co-transfected with 8 μg of rat brain β_{2a}[35], 8 μg of rat brain $\alpha_{2\delta}$[36], and 1–8 μg of Ca^{2+} channel α_1 subunit. All α_{1C} and α_{1D} constructs were co-transfected with 2 μg of SV40 T antigen to enhance expression; 8 μg of cDNA for rat brain CaM_{12}, CaM_{34}, or CaM_{1234} was added as required[20].

Room temperature, whole-cell recordings were performed 1–3 days after transfection, using Axopatch 200A/B amplifiers (Axon Instruments). P/8 leak subtraction was used, with series resistances of 1–2 MΩ after >70% compensation. Currents were filtered at 2 kHz (4-pole Bessel), and sampled at 10 kHz. For high-buffer experiments, internal solutions contained, (in mM): $CsMeSO_3$, 114; $CsCl_2$, 5; $MgCl_2$, 1; MgATP, 4; HEPES (pH 7.4), 10; and BAPTA, 10; at 295 mOsm adjusted with $CsMeSO_3$. For low-buffer experiments, (in mM): $CsMeSO_3$, 135; $CsCl_2$, 5; $MgCl_2$, 1; MgATP, 4; HEPES (pH 7.4), 10; and EGTA, 0.5. In all experiments, except those with $Ca_V1.2/1.3$, external solutions contained (in mM): TEA-$MeSO_3$, 140; HEPES (pH 7.4), 10; and $CaCl_2$ or $BaCl_2$, 5; at 300 mOsm, adjusted with TEA-$MeSO_3$. Due to lower $Ca_V1.2$ expression, 20 mM $CaCl_2$ or $BaCl_2$ was used during high internal buffering, and 10 mM during low buffering. $Ca_V1.3$ recordings were made in 40 mM $CaCl_2$ or $BaCl_2$. A holding potential of −90 mV and 60 s repetition interval were used throughout. Data were analyzed by custom MATLAB software (Mathworks, MA), with average data shown as mean ± SEM.

FRET two-hybrid assay

Fluorescence resonance energy transfer (FRET) two-hybrid experiments were carried out in HEK293 cells and analyzed as described[13]. During imaging, the bath solution was a Tyrode's buffer containing 10 mM Ca^{2+}, where 5 μM ionomycin (Sigma-Aldrich, MO) was added for Ca^{2+}/CaM experiments. Concentration-dependent spurious FRET was subtracted from the raw data prior to binding-curve analysis[37].

Gel mobility shift assay

We used a non-denaturing, 13% acrylamide resolving gel, coupled with a 4% acrylamide stacking gel. 100 μM $CaCl_2$ was added to the gel to maintain Ca^{2+}/CaM binding. Peptide samples were freshly solubilized into a sample buffer: 20 mM Tris-Cl (pH=6.8), 150 mM NaCl, 2% glycerol, 10 mM $CaCl_2$, 0.001% bromphenol blue dye, and 2 μg purified CaM protein[7]. Binding reactions (×1h) and electrophoresis were performed at ~0–4°C in 25 mM Tris (pH=8.4) and 200 mM glycine, with parameters of 50 V × 20 min, followed by 100 V × 2 h. Gels were stained over heat × 1 h with Commassie R-250 (Bio-Rad Laboratories, CA),

and destained overnight[20]. Peptides were synthesized by the Synthesis and Sequencing Facility at the Johns Hopkins School of Medicine (Baltimore, MD). The wildtype *NSCaTE* peptide $NT_{C\text{-peptide}}$ was SWQAAIDAARQAKLMGS (rabbit α_{1C} sequence), and the mutant was SAQAAIDAARQAKLMGS. The IQ_A peptide was KIYAAMMIMEYYRQSKAKKLQ (based on human α_{1A} subunit[2]). IQ_A peptide was added to Ca^{2+}/CaM in a molar ratio of 8:1 to produce a maximal binding shift. *NSCaTE* peptide was then added in varying amounts (Fig. 2a).

Dansyl CaM experiments

Purified recombinant CaM protein was dansylated with 0.5 mM dansyl-Cl under alkaline conditions at room temperature (0.3 mM $CaCl_2$ × 4 hours). The reaction was terminated with 5 mM hydroxylamine, and Tris buffer added before dialysis against 10 mM MOPS (pH 7.2) at 4°C[38]. Peptides were as above. Spectrofluorometry was conducted at 25°C in 5 mM $CaCl_2$, 150 mM NaCl, and 50 mM Tris-Cl (pH=7.5). Peptide stocks were freshly prepared and used within 6 h. 100 nM dansyl-CaM was excited at 340 nm, and fluorescence recorded from 400–650 nm (slit size, 3 nm excitation, 15 nm emission; integration time, 0.1 s), using a Fluorolog-3 spectrofluorometer (Horiba Jobin Yvon). No detectable bleaching was observed in controls. Binding curves were determined from the average of five 490-nm measurements (F_{490}) at each peptide concentration. Subtraction of background fluorescence utilized a correction factor (m_{peptide}) derived from measurements of peptide alone ($F_{490,\text{bg-corrected}} = F_{490} - m_{\text{peptide}} \cdot [\text{peptide}]$). We calculated $F_{490,\text{full-corrected}} = F_{490,\text{bg-corrected}} \cdot V_{\text{tot}} / V_{\text{initial}}$ (where V_{tot} is the final volume, and V_{initial} was 2.5 mL), so as to correct for dilution by successive peptide additions. Fractional binding (B) was $(F_{490,\text{full-corrected,max}} - F_{490,\text{full-corrected}}) / (F_{490,\text{full-corrected,max}} - F_{490,\text{full-corrected,min}})$; least-square fits were performed using $B = [\text{peptide}]^k / ([\text{peptide}]^k + K_d^k)$, with resulting $k \sim 1$.

Supplementary Material

Refer to Web version on PubMed Central for supplementary material.

Acknowledgements

We thank Drs. Heather Agler and Masayuki Mori for early characterization of the cBBBBb chimeric channel, Drs. Carrie Iwema and Jonathan Pevsner for bioinformatics advice; King-Wai Yau, Eric Young, and members of the CSL lab for valuable comments. Supported by grants from the NINDS (to I.E.D.), NIGMS (to M.R.T.), and from the NIMH and NHLBI (to D.T.Y.)

References

1. Lee A, Scheuer T, Catterall WA. Ca2+/calmodulin-dependent facilitation and inactivation of P/Q-type Ca2+ channels. J Neurosci. 2000; 20:6830–6838. [PubMed: 10995827]
2. DeMaria CD, Soong TW, Alseikhan BA, Alvania RS, Yue DT. Calmodulin bifurcates the local Ca2+ signal that modulates P/Q-type Ca2+ channels. Nature. 2001; 411:484–489. [PubMed: 11373682]
3. Liang H, et al. Unified mechanisms of Ca2+ regulation across the Ca2+ channel family. Neuron. 2003; 39:951–960. [PubMed: 12971895]
4. Bootman MD, Lipp P, Berridge MJ. The organisation and functions of local Ca(2+) signals. J Cell Sci. 2001; 114:2213–2222. [PubMed: 11493661]

5. Evans RM, Zamponi GW. Presynaptic Ca2+ channels--integration centers for neuronal signaling pathways. Trends Neurosci. 2006; 29:617–624. [PubMed: 16942804]
6. Dunlap K. Calcium channels are models of self-control. J Gen Physiol. 2007; 129:379–383. [PubMed: 17438121]
7. Alseikhan BA, DeMaria CD, Colecraft HM, Yue DT. Engineered calmodulins reveal the unexpected eminence of Ca2+ channel inactivation in controlling heart excitation. Proc Natl Acad Sci U S A. 2002; 99:17185–17190. [PubMed: 12486220]
8. Xu J, Wu LG. The decrease in the presynaptic calcium current is a major cause of short-term depression at a calyx-type synapse. Neuron. 2005; 46:633–645. [PubMed: 15944131]
9. Dolmetsch RE, Pajvani U, Fife K, Spotts JM, Greenberg ME. Signaling to the nucleus by an L-type calcium channel-calmodulin complex through the MAP kinase pathway. Science. 2001; 294:333–339. [PubMed: 11598293]
10. Mori MX, Erickson MG, Yue DT. Functional stoichiometry and local enrichment of calmodulin interacting with Ca2+ channels. Science. 2004; 304:432–435. [PubMed: 15087548]
11. Yang PS, Mori MX, Antony EA, Tadross MR, Yue DT. A single calmodulin imparts distinct N- and C-lobe regulatory processes to individual $Ca_V1.3$ channels (abstr.). Biophys. J. 2007; 354a(Supplement) 1669-Platform.
12. Pitt GS, et al. Molecular basis of calmodulin tethering and Ca2+-dependent inactivation of L-type Ca2+ channels. J Biol Chem. 2001; 276:30794–30802. [PubMed: 11408490]
13. Erickson MG, Liang H, Mori MX, Yue DT. FRET two-hybrid mapping reveals function and location of L-type Ca^{2+} channel CaM preassociation. Neuron. 2003; 39:97–107. [PubMed: 12848935]
14. Yang PS, et al. Switching of Ca2+-dependent inactivation of Ca(v)1.3 channels by calcium binding proteins of auditory hair cells. J Neurosci. 2006; 26:10677–10689. [PubMed: 17050707]
15. Augustine GJ, Santamaria F, Tanaka K. Local calcium signaling in neurons. Neuron. 2003; 40:331–346. [PubMed: 14556712]
16. Neher E. Vesicle pools and Ca^{2+} microdomains: new tools for understanding their roles in neurotransmitter release. Neuron. 1998; 20:389–399. [PubMed: 9539117]
17. Chaudhuri D, Issa JB, Yue DT. Elementary Mechanisms Producing Facilitation of Cav2.1 (P/Q-type) Channels. J Gen Physiol. 2007; 129:385–401. [PubMed: 17438119]
18. Song LS, Sham JS, Stern MD, Lakatta EG, Cheng H. Direct measurement of SR release flux by tracking 'Ca^{2+} spikes' in rat cardiac myocytes. J. Physiol. (Lond.). 1998; 512:677–691. [PubMed: 9769413]
19. Tadross MR, Dick IE, Yue DT. Mechanism of Ca^{2+} decoding by the CaM/Ca_V channel complex (abstr.). Biophys. J. 2007; (Supplement):354a. 1670-Plat.
20. Peterson BZ, DeMaria CD, Adelman JP, Yue DT. Calmodulin is the Ca2+ sensor for Ca2+ -dependent inactivation of L-type calcium channels. Neuron. 1999; 22:549–558. [PubMed: 10197534]
21. Tang ZZ, et al. Transcript scanning reveals novel and extensive splice variations in human l-type voltage-gated calcium channel, $Ca_v1.2$ alpha1 subunit. J Biol Chem. 2004; 279:44335–44343. [PubMed: 15299022]
22. Van Petegem F, Chatelain FC, Minor DL Jr. Insights into voltage-gated calcium channel regulation from the structure of the CaV1.2 IQ domain-Ca2+/calmodulin complex. Nat Struct Mol Biol. 2005; 12:1108–1115. [PubMed: 16299511]
23. Ivanina T, Blumenstein Y, Shistik E, Barzilai R, Dascal N. Modulation of L-type Ca^{2+} channels by gbeta gamma and calmodulin via interactions with N and C termini of alpha 1C. J Biol Chem. 2000; 275:39846–39854. [PubMed: 10995757]
24. de Leon M, et al. Essential Ca(2+)-binding motif for Ca(2+)-sensitive inactivation of L-type Ca2+ channels. Science. 1995; 270:1502–1506. [PubMed: 7491499]
25. Rhoads AR, Friedberg F. Sequence motifs for calmodulin recognition. FASEB J. 1997; 11:331–340. [PubMed: 9141499]
26. Toescu EC, Verkhratsky A. The importance of being subtle: small changes in calcium homeostasis control cognitive decline in normal aging. Aging Cell. 2007; 6:267–273. [PubMed: 17517038]

27. Moosmang S, et al. Role of hippocampal Cav1.2 Ca2+ channels in NMDA receptor-independent synaptic plasticity and spatial memory. J Neurosci. 2005; 25:9883–9892. [PubMed: 16251435]

28. Evans J, Erickson MG, Anderson MJ, Yue DT. FRET-based mapping of calmodulin preassociation with P/Q-type Ca channels (abstr.). Biophys J. 2003; (Supplement) 2615-Pos.

29. Kobrinsky E, Schwartz E, Abernethy DR, Soldatov NM. Voltage-gated mobility of the Ca2+ channel cytoplasmic tails and its regulatory role. J Biol Chem. 2003; 278:5021–5028. [PubMed: 12473653]

30. Drum CL, et al. Structural basis for the activation of anthrax adenylyl cyclase exotoxin by calmodulin. Nature. 2002; 415:396–402. [PubMed: 11807546]

references below in Methods

31. Agler HL, et al. G protein-gated inhibitory module of N-type ($Ca_V2.2$) Ca^{2+} channels. Neuron. 2005; 46:891–904. [PubMed: 15953418]

32. Xu W, Lipscombe D. Neuronal Ca(V)1.3alpha(1) L-type channels activate at relatively hyperpolarized membrane potentials and are incompletely inhibited by dihydropyridines. J Neurosci. 2001; 21:5944–5951. [PubMed: 11487617]

33. Williams ME, et al. Structure and functional expression of an omega-conotoxin- sensitive human N-type calcium channel. Science. 1992; 257:389–395. [PubMed: 1321501]

34. Wei XY, et al. Heterologous regulation of the cardiac Ca^{2+} channel alpha 1 subunit by skeletal muscle beta and gamma subunits. Implications for the structure of cardiac L-type Ca^{2+} channels. J. Biol. Chem. 1991; 266:21943–21947. [PubMed: 1718988]

35. Perez-Reyes E, et al. Cloning and expression of a cardiac/brain beta subunit of the L- type calcium channel. J. Biol. Chem. 1992; 267:1792–1797. [PubMed: 1370480]

36. Tomlinson WJ, et al. Functional properties of a neuronal class C L-type calcium channel. Neuropharmacology. 1993; 32:1117–1126. [PubMed: 8107966]

37. Stratton J, Evans J, Erickson MG, Alvania RS, Yue DT. The nature of concentration-dependent spurious FRET arising from CFP and YFP (abstr.). Biophys J. 2004; 86:317a.

38. Kincaid RL, Billingsley ML, Vaughan M. Preparation of fluorescent, cross-linking, and biotinylated calmodulin derivatives and their use in studies of calmodulin-activated phosphodiesterase and protein phosphatase. Methods Enzymol. 1988; 159:605–626. [PubMed: 2842624]

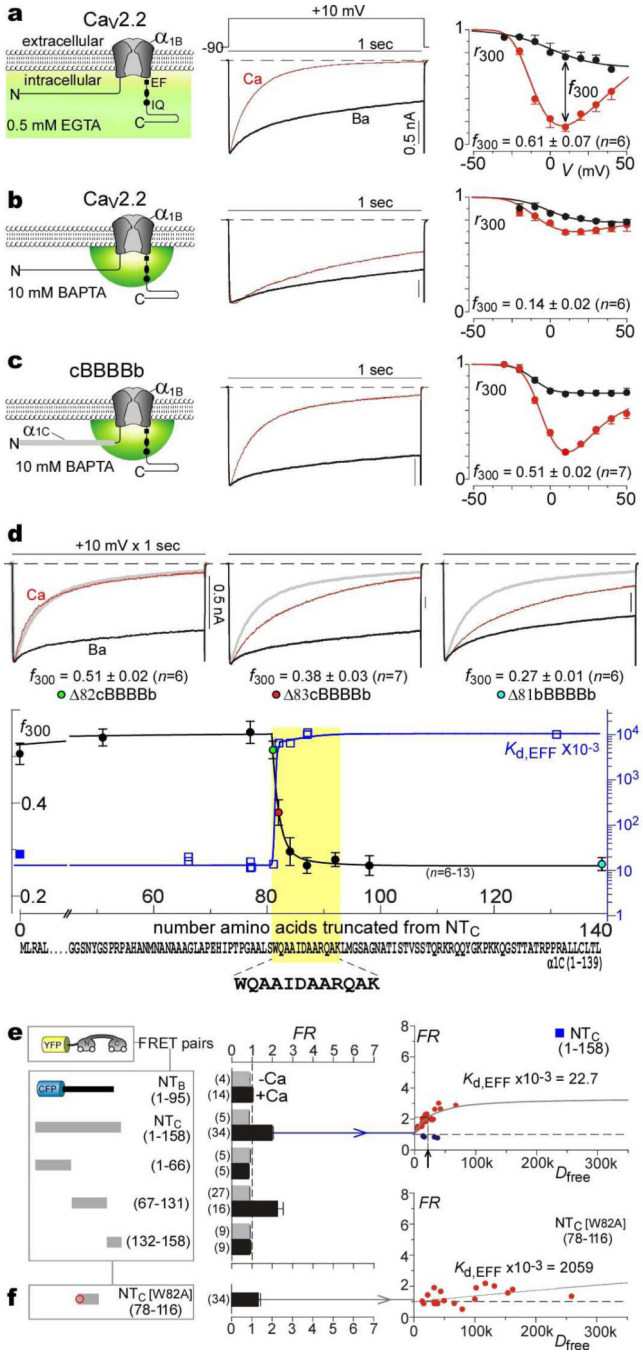

Figure 1. Transformation of spatial Ca^{2+} selectivity in $Ca_V2.2$ channels

a, $Ca_V2.2$ CDI, low buffering. Left, cartoon of global Ca^{2+} elevation. Middle, exemplar traces in Ca^{2+} (red) and Ba^{2+} (black). Throughout, current bar references Ca^{2+} trace; Ba^{2+} trace normalized to Ca^{2+} peak. Right, average CDI; f_{300} at 10 mV; data, mean ± SEM throughout; cell number in parentheses. **b**, $Ca_V2.2$ CDI, high buffering. Left, cartoon of local Ca^{2+} signaling. **c**, CDI of cBBBBb. **d**, Localizing spatial Ca^{2+} transforming element (yellow highlight) within NT_C. Top, exemplar currents for cBBBBb with amino-terminal deletions, (Δ82cBBBBb, removal of first 81 aa of cBBBBb; Δ81bBBBBb, removal of entire

amino terminus of $Ca_V2.2$). Bottom, f_{300} (high buffering) versus residues deleted from cBBBBb; left axis and circles with colors corresponding to exemplars above. $K_{d,EFF}$ is also plotted on same abscissa; blue right axis and blue squares, with filled symbol corresponding to **e**. Extreme bottom, localized sequence for both CDI transformation and Ca^{2+}/CaM binding within NT_C (yellow highlight).

e, f, FRET for YFP–CaM versus channel amino-terminal segments tagged with CFP. Left, construct schematics. Middle, FRET ratios (*FR*). Right, exemplar binding curves, with red symbols for Ca^{2+}/CaM, and blue symbols for apoCaM (e, arrow shows $K_{d,EFF}$).

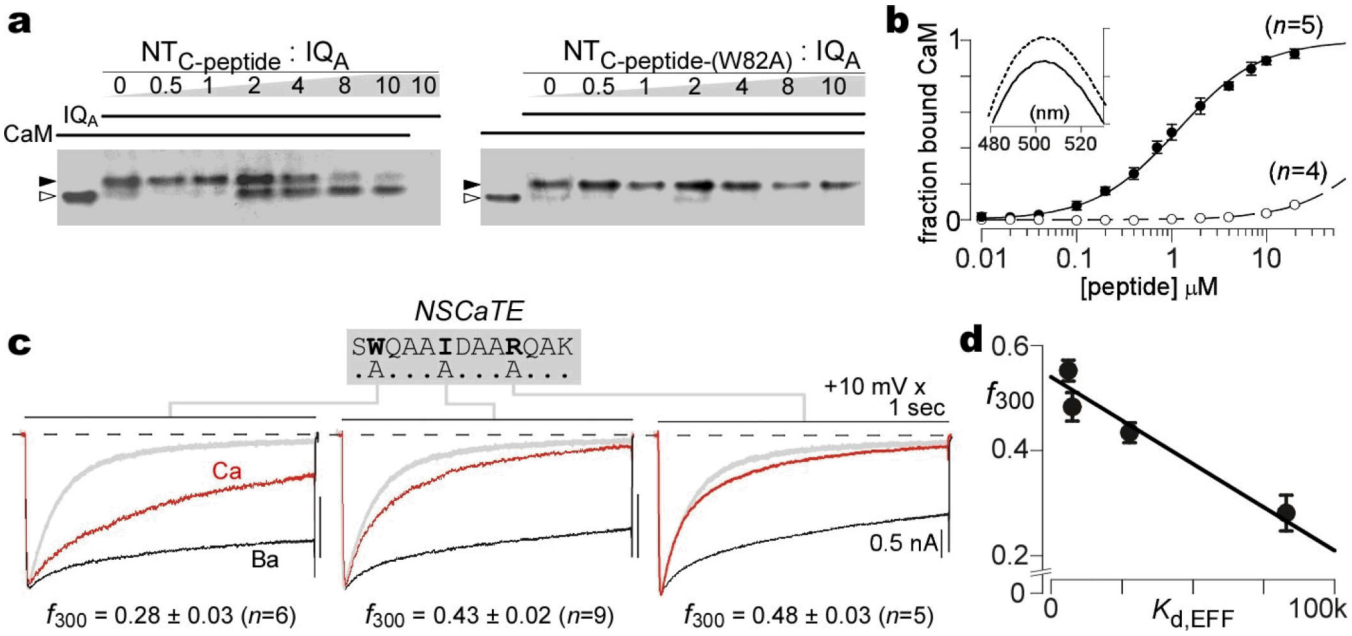

Figure 2. Direct CaM binding and mapping of key *NSCaTE* residues

a, Competitive gel mobility shift assay, confirming Ca^{2+}/CaM interaction with $NT_{C\text{-}peptide}$ (left), not mutant $NT_{C\text{-}peptide\text{-}(W82A)}$ (right). **b**, Dansylated Ca^{2+}/CaM spectrofluorometry. Binding with $NT_{C\text{-}peptide}$ (filled circles), not with mutant $NT_{C\text{-}peptide\text{-}(W82A)}$ (open circles), both plotted as mean ± SEM. Inset, $NT_{C\text{-}peptide}$ decreases emission spectrum. **c**, CDI in high buffering, for Δ78cBBBBb channels with point mutations as labeled. Format as in Fig. 1a; gray trace shows baseline Δ78cBBBBb profile. **d**, Close correlation of CDI in high buffering with NT_C module affinity for Ca^{2+}/CaM_{34} (Supplemmentary Information 2.1).

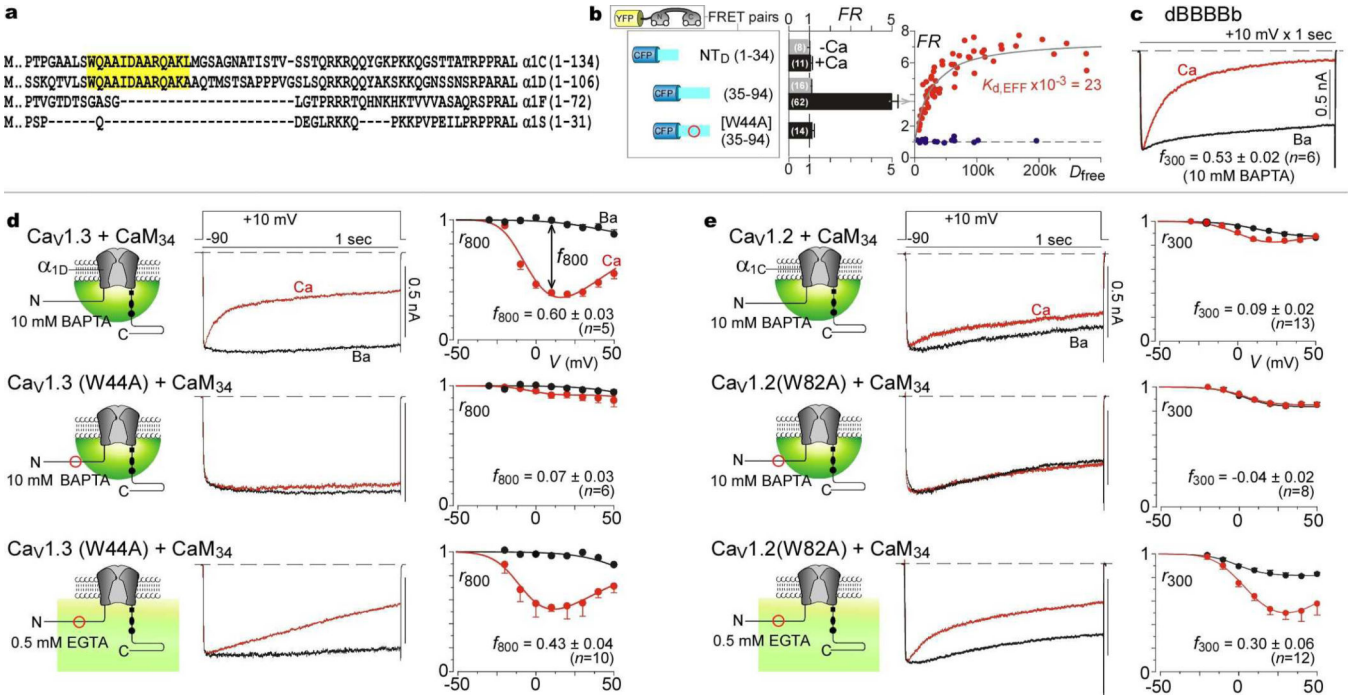

Figure 3. *NSCaTE* transforms spatial Ca^{2+} selectivity in native Ca_V1 channels

a, α_1 alignment, Ca_V1 channels. **b**, FRET assays. Format as in Fig. 1e. **c**, CDI of dBBBBb in high buffering. **d**, Impact of native *NSCaTE* upon N-lobe CDI of $Ca_V1.3$. Top, CDI persists in high buffering. Middle, CDI elimination by W44A mutation. Bottom, CDI reappearance in W44A mutant under low buffering. Format as in Fig. 1a, except for 800-msec metrics. **e**, Native *NSCaTE* effects in $Ca_V1.2$. Format as in **d**, with 300-msec metrics.

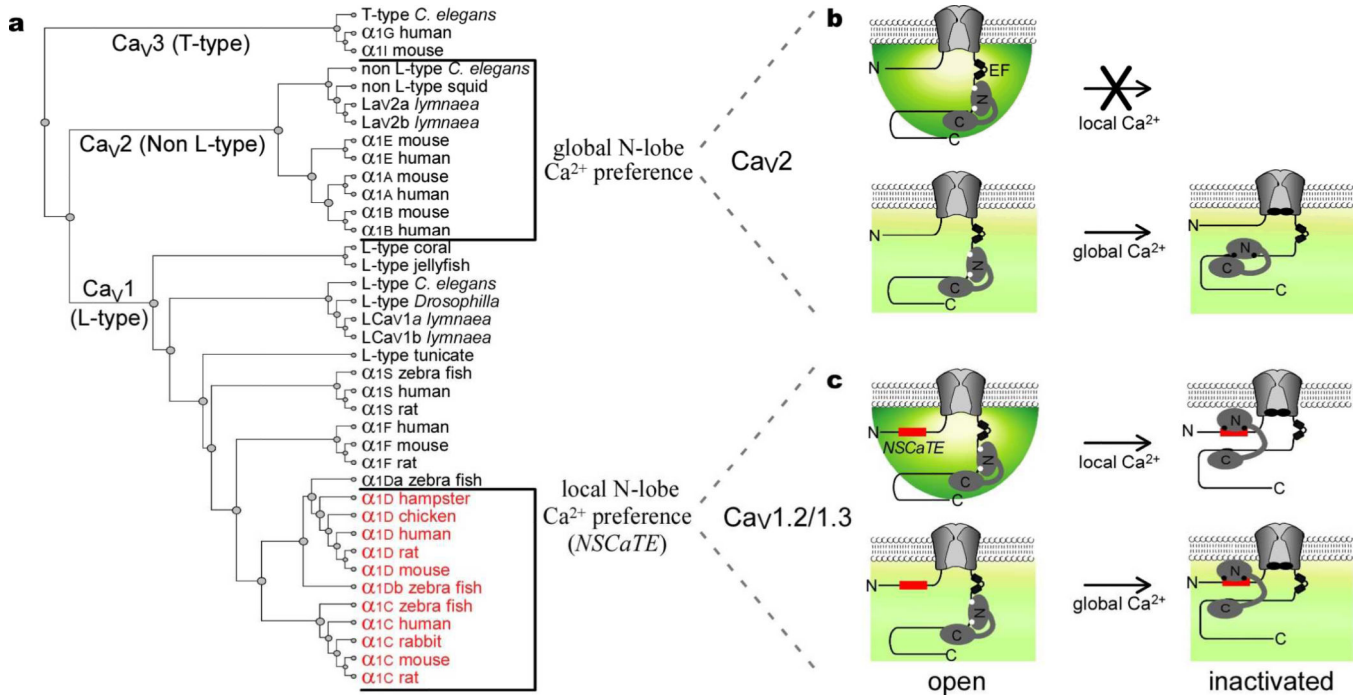

Figure 4. Functional and structural properties for *NSCaTE* switching of spatial Ca^{2+} selectivity

a, Ca_V1-2 dendrogram, based on α_1 subunits (Supplementary Information 4.1). Red, *NSCaTE*-containing channels. **b**, Schematic of N-lobe CDI in Ca_V2 channels. Absence of *NSCaTE* yields global Ca^{2+} selectivity. Black circles on CaM, Ca^{2+} ions. **c**, N-lobe CDI in Ca_V1 channels that contain *NSCaTE* (red) exhibit local Ca^{2+} selectivity. CaM bridges amino and carboxy termini of inactivated channels (right).